

Quantum Dynamics of Attractive and Repulsive Polarons in a Doped MoSe₂ Monolayer

Di Huang¹, Kevin Sampson¹, Yue Ni¹, Zhida Liu¹, Danfu Liang³, Kenji Watanabe⁶, Takashi Taniguchi⁷, Hebin Li³, Eric Martin⁵, Jesper Levinsen², Meera M. Parish², Emanuel Tutuc⁴, Dmitry K. Efimkin², and Xiaoqin Li^{1,*}

¹*Department of Physics and Center for Complex Quantum Systems,
The University of Texas at Austin, Austin, Texas 78712, USA*

²*School of Physics and Astronomy and ARC Centre of Excellence in Future Low-Energy Electronics
Technologies, Monash University, Victoria 3800, Australia*

³*Department of Physics, Florida International University, Miami, Florida 33199, USA*

⁴*Microelectronics Research Center, Department of Electrical and Computer Engineering,
The University of Texas at Austin, Austin, Texas 78712, USA*

⁵*MONSTR Sense Technologies, LLC, Ann Arbor, Michigan, 48104, USA*

⁶*Research Center for Functional Materials, National Institute for Materials Science,
1-1 Namiki, Tsukuba 305-0044, Japan*

⁷*International Center for Materials Nanoarchitectonics, National Institute for Materials Science,
1-1 Namiki, Tsukuba 305-0044, Japan*

 (Received 17 July 2022; revised 12 November 2022; accepted 23 January 2023; published 2 March 2023)

When mobile impurities are introduced and coupled to a Fermi sea, new quasiparticles known as Fermi polarons are formed. There are two interesting, yet drastically different regimes of the Fermi polaron problem: (i) the attractive polaron (AP) branch connected to pairing phenomena spanning the crossover from BCS superfluidity to the Bose-Einstein condensation of molecules and (ii) the repulsive branch (RP), which underlies the physics responsible for Stoner's itinerant ferromagnetism. Here, we study Fermi polarons in two-dimensional systems, where many questions and debates regarding their nature persist. The model system we investigate is a doped MoSe₂ monolayer. We find the observed AP-RP energy splitting and the quantum dynamics of attractive polarons agree with the predictions of polaron theory. As the doping density increases, the quantum dephasing of the attractive polarons remains constant, indicative of stable quasiparticles, while the repulsive polaron dephasing rate increases nearly quadratically. The dynamics of Fermi polarons are of critical importance for understanding the pairing and magnetic instabilities that lead to the formation of rich quantum phases found in a wide range of physical systems including nuclei, cold atomic gases, and solids.

DOI: [10.1103/PhysRevX.13.011029](https://doi.org/10.1103/PhysRevX.13.011029)

Subject Areas: Condensed Matter Physics, Optics,
Semiconductor Physics

I. INTRODUCTION

Fermi-polaron quasiparticles are mobile impurities (e.g., excitons) that are coherently dressed by density fluctuations (particle-hole excitations) of a surrounding Fermi sea [1,2]. As illustrated in Fig. 1(a), the attractive interaction between the exciton and Fermi sea leads to an energetically favorable state—the attractive polaron—as well as a higher-energy repulsive polaron, a metastable state that eventually decays into attractive polarons. The behavior of Fermi polarons has been extensively studied in the context of

ultracold atomic gases, where experiments have probed the formation of polarons [3] as well as their quasiparticle properties, such as the polaron energy [4], lifetime [5], and the effective mass [6]. However, cold-atom experiments have focused on three-dimensional systems. Intriguing and open questions remain, e.g., how the Fermi polarons evolve as the dimensionality is lowered and low-energy density fluctuations of the Fermi sea are enhanced. In one-dimensional systems, the impurity problem becomes exactly solvable [7], and polaronic quasiparticles are destroyed by quantum fluctuations. Thus, the intermediate case of two-dimensional (2D) systems represents a particularly interesting yet unresolved case, where quantum fluctuations are enhanced but quasiparticles can still exist.

Atomically thin transition-metal dichalcogenides (TMDCs) represent exemplary 2D systems to study the rich properties of Fermi polarons, where an exciton is dressed by Fermi seas with a unique valley degree of

*elaineli@physics.utexas.edu

Published by the American Physical Society under the terms of the [Creative Commons Attribution 4.0 International license](https://creativecommons.org/licenses/by/4.0/). Further distribution of this work must maintain attribution to the author(s) and the published article's title, journal citation, and DOI.

freedom [8,9]. A variety of exciton resonances (neutral or charged states, biexcitons, spatial and momentum-space indirect excitons) have been identified and investigated in TMDC monolayers [10,11]. The trion, a three-body bound state consisting of an exciton bound to an extra electron or hole, has been used widely in the literature to describe an optical resonance appearing at an energy of approximately 20–30 meV below the neutral excitons [12]. The trion picture is difficult to distinguish from the polaron picture at low doping densities, where the Fermi energy is smaller than the intrinsic exciton linewidth [13–16]. However, as doping increases, a continuous energy shift suggests that the three-body bound-state picture is insufficient [17–19]. Attractive and repulsive polarons (APs and RPs), as illustrated in Fig. 1(b), have been proposed to explain the evolution of reflectivity spectra of doped TMDC monolayers and bilayers with doping [8,20]. This polaron picture is anticipated to be relevant up to moderate doping, where the interelectron distance is sufficiently large compared to the radii of photoexcited excitons such that their formation is not disturbed. A critical question remains:

Does polaron theory predict different properties of APs and RPs? Quantum decoherence associated with APs and RPs, for example, has never been investigated experimentally, and a comparison between experiments and theory has not been possible so far.

Here, we study the emergence and evolution of APs and RPs in a MoSe₂ monolayer as the electron doping density increases. Using two-dimensional coherent electronic spectroscopy (2DCES), we follow the changes in resonant energy, oscillator strength, and quantum decoherence of the AP and RP branches. The observed redshift of the AP resonance suggest that these new quasiparticles are energetically stable. The redshift increases until a critical doping density is reached, and a more pronounced blueshift occurs. Intriguingly, the quantum decoherence rate of APs (measured via the homogeneous linewidth) remains nearly constant up to a critical density, which suggests that the excitons are coherently dressed by the Fermi sea. The quantum decoherence rate of RPs, however, increases monotonically and rapidly with doping density. Our study highlights that optically excited TMDCs represent a novel

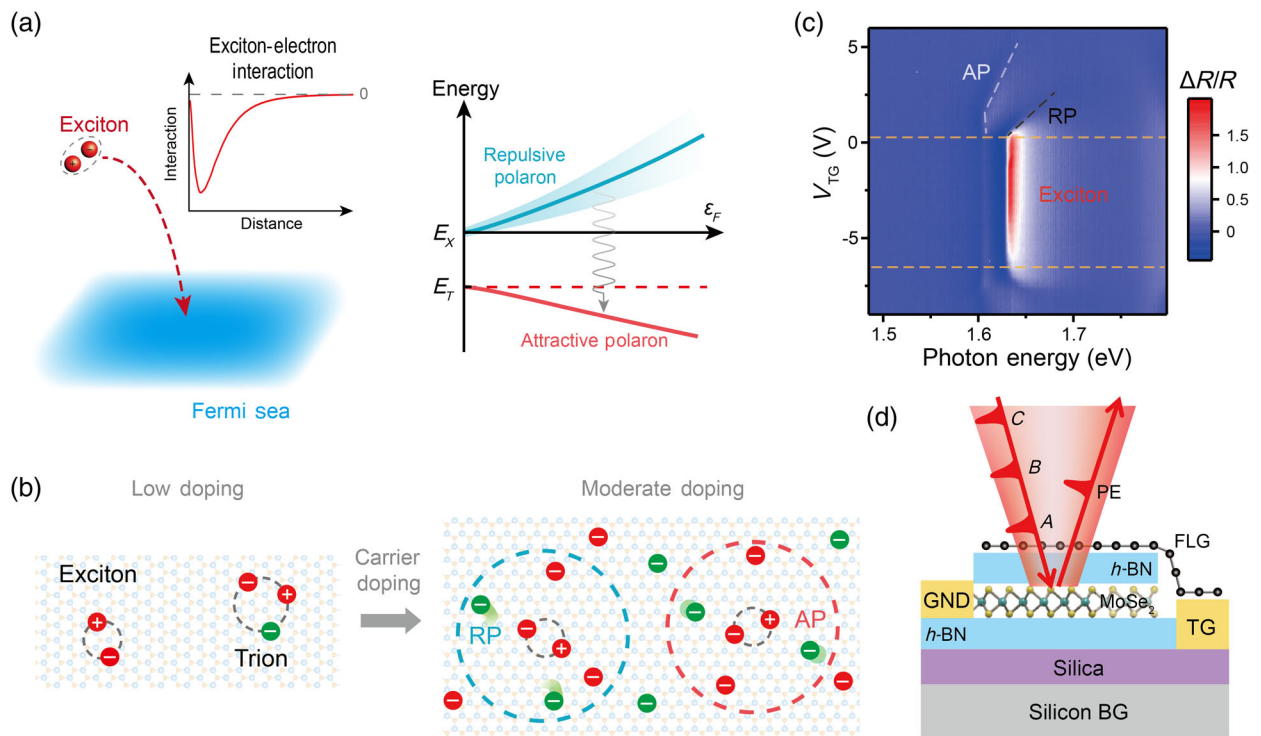


FIG. 1. Illustration of the MoSe₂ device and physical concept. (a) Schematic of Fermi polarons. When excitons are attractively coupled to a Fermi sea of electrons, the spectrum of the whole system splits into two branches: APs and RPs. In the limit of vanishing Fermi energy ϵ_F , the APs and RPs recover the energies of trions (E_T) and excitons (E_X), respectively. (b) Evolution from an exciton-trion picture to a Fermi-polaron picture as the doping density increases in a monolayer. Spheres in red refer to electrons (−) and holes (+) in one valley, while spheres in green color indicate the opposite valley. The displacement of electrons around the exciton in the moderate-doping regime represents the polaronic cloud of density fluctuations (particle-hole excitations). (c) Reflectance spectra from a doped MoSe₂ monolayer at different top-gate voltages (V_{TG}). The dashed lines are guidelines for the evolution of APs (bright) and RPs (dark). (d) Schematics of a collinear 2DCES experiment performed on a monolayer MoSe₂ device. A train of three pulses (A, B, C) is focused onto the monolayer MoSe₂, and the photon-echo (PE) signal is collected via the same microscope objective. The pulses are incident perpendicular to the sample but are illustrated here at an angle for clarity.

playground to study the rich phenomenology of strongly imbalanced quantum mixtures.

II. RESULTS

We control the doping density in a MoSe₂ monolayer encapsulated between hexagonal boron nitride (*h*-BN) layers using a device with a few-layer graphite top gate (TG) and a silicon back gate (BG) (details in Supplemental Material [21]). All optical measurements are taken at 16 K unless stated otherwise. We first measure reflectance spectra at different doping levels, as shown in Fig. 1(c). When the MoSe₂ monolayer is charge neutral or in the regime of dilute doping density (between the two orange dashed lines), two

resonances at 1635 and 1605 meV are attributed to excitons and trions, respectively. We focus on the electron doping regimes with positive TG voltages. The exciton resonance evolves into the RP branch, which exhibits a blueshift at $V_{\text{TG}} > 0.5$ V. The lower-energy resonance exhibits a small redshift for $V_{\text{TG}} = 0.5\text{--}1.5$ V before a pronounced blueshift starts to occur at $V_{\text{TG}} > 1.5$ V.

In the following, we analyze the spectral shift, oscillator strength changes, and quantum dephasing of these resonances using 2DCES. As illustrated in Fig. 1(d), three collinearly polarized ultrafast pulses derived from the same laser are focused onto the sample by a microscope objective. The third-order optical nonlinear response leads to a coherent photon-echo signal, which is collected by the

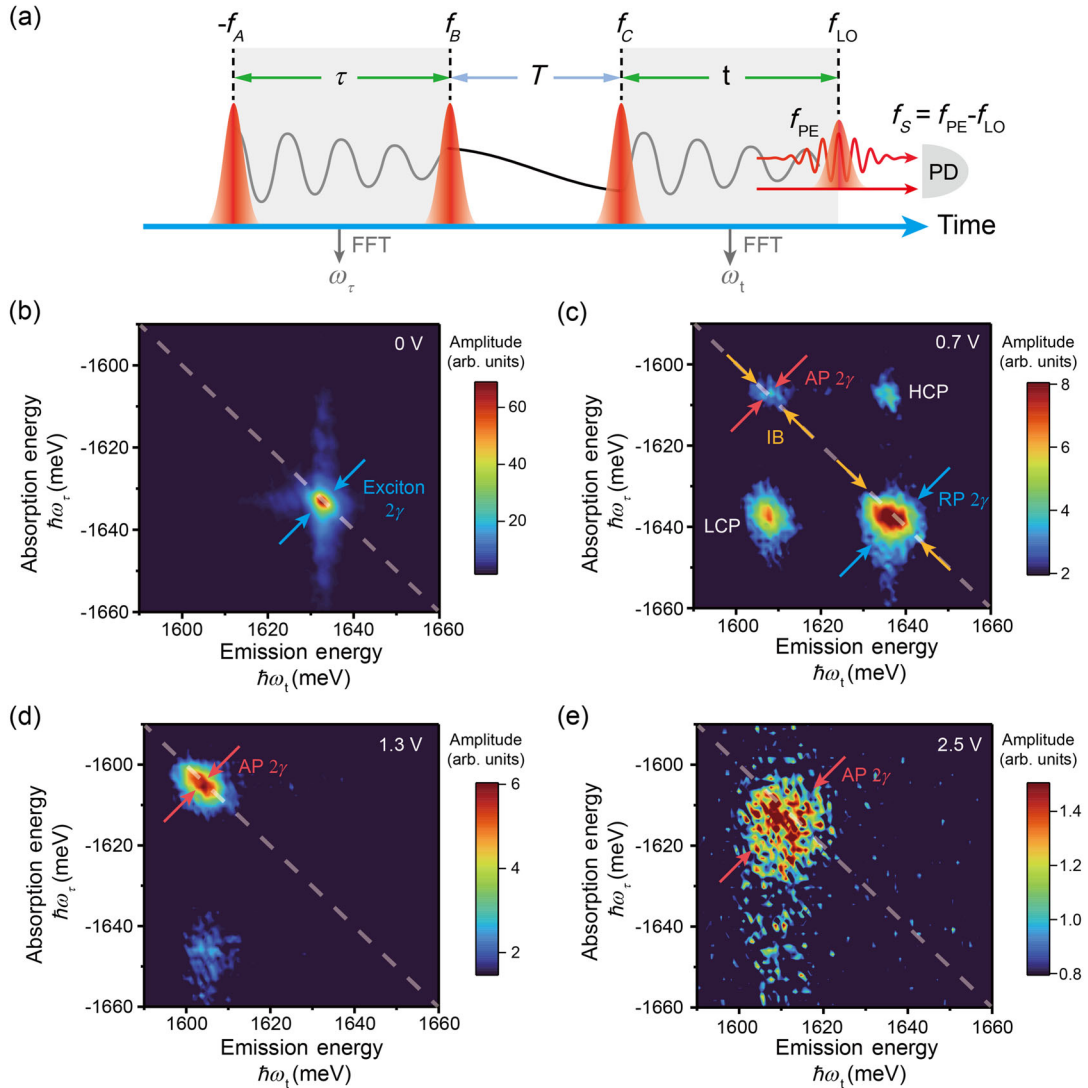


FIG. 2. One-quantum rephasing amplitude spectra of the MoSe₂ monolayer at different gate voltages. (a) Schematic of the one-quantum rephasing pulse sequence. Details are further discussed in the Supplemental Material [21]. (b)–(e) 2D spectra taken at different top-gate voltages at 0, 0.7, 1.3, and 2.5 V, respectively. These gate voltages correspond to estimated electron doping densities of $n_{e^-} = 0, 6.6 \times 10^{11}, 2.6 \times 10^{12},$ and $6.6 \times 10^{12} \text{ e}^-/\text{cm}^2$. IB, inhomogeneous broadening; HCP and LCP, higher and lower off-diagonal cross peak. Homogeneous (inhomogeneous) linewidth of exciton, AP, and RP could be extracted by fitting the cross-diagonal (diagonal) slices of the spectra, as illustrated by the arrows in blue (exciton and RP) and red (AP) color.

same objective, isolated, and detected using a frequency-modulation scheme after the heterodyne detection with a reference pulse (details in Supplemental Material [21]). The laser spectrum covers both the AP and RP resonances identified in the reflectance spectrum, and resonantly excites them.

We perform one-quantum rephasing measurements in which the time delays between the first two excitation pulses (τ) and that between the third pulse and a reference pulse (t) are scanned, as illustrated in Fig. 2(a). These two time delays (τ and t) are then Fourier transformed to yield the absorption energy ($\hbar\omega_r$) and emission energy ($\hbar\omega_e$), respectively. The waiting time T between the second and third pulses is kept at 100 fs to avoid artifacts that occur during the temporal overlap between the excitation pulses. The amplitude of the photon-echo signal as a correlation between absorption and emission frequencies is shown in Figs. 2(b)–2(e). The elongation along the diagonal direction indicated by the dashed line is determined by the inhomogeneous linewidth, while the full width at half maximum along the cross diagonal direction indicated by two arrows reveals the homogeneous linewidth 2γ [22], where γ is the decoherence rate and inversely proportional to the quantum dephasing time $1/T_2 = \gamma/\hbar$.

We further investigate the one-quantum spectra of monolayer MoSe₂ at several doping levels in Figs. 2(b)–2(e). In the charge-neutral regime up to $V_{\text{TG}} = 0.5$ V, the spectrum is dominated by the exciton resonance at approximately

1633 meV [23,24]. At the carrier density of $n = 6.6 \times 10^{11} e^-/\text{cm}^2$ (or $V_{\text{TG}} = 0.7$ V), both AP and RP are observed as two diagonal peaks appearing at approximately 1605 and 1637 meV, respectively. Moreover, two off-diagonal cross peaks emerge, which are labeled as the lower and higher cross peak (i.e., LCP and HCP). These cross peaks result from electronic coupling between the APs and RPs as previously studied in the nominally doped MoSe₂ monolayers [25]. The unbalanced LCP and HCP intensities originate from both coherent quantum beats and decays from RP to AP. Upon further increasing the doping density to $n = 2.6 \times 10^{12} e^-/\text{cm}^2$ ($V_{\text{TG}} = 1.3$ V), the spectral weight has nearly completely shifted to APs. A weak LCP peak remains in the spectrum, suggesting that the metastable RPs still absorb light but quickly decay to APs. At the highest doping density $n = 6.6 \times 10^{12} e^-/\text{cm}^2$ ($V_{\text{TG}} = 2.5$ V) where a nonlinear signal is still detectable, the AP resonance becomes much broader and shifts to higher energy.

We carefully analyze the energy shifts and quantum decoherence rates of APs and RPs extracted from 2D spectra as shown in Fig. 3. The slices along the cross-diagonal direction for the RPs and APs peak at a few selected TG voltages are displayed in Figs. 3(a) and 3(b), respectively. The homogeneous linewidth of the RP rapidly increases with electron doping density ($\gamma = 1.03 \pm 0.09$ and 2.50 ± 0.30 meV with $V_{\text{TG}} = 0$ and 0.7 V, respectively) corresponding to a higher decoherence rate as summarized in Fig. 3(c) (blue curve). By contrast, the

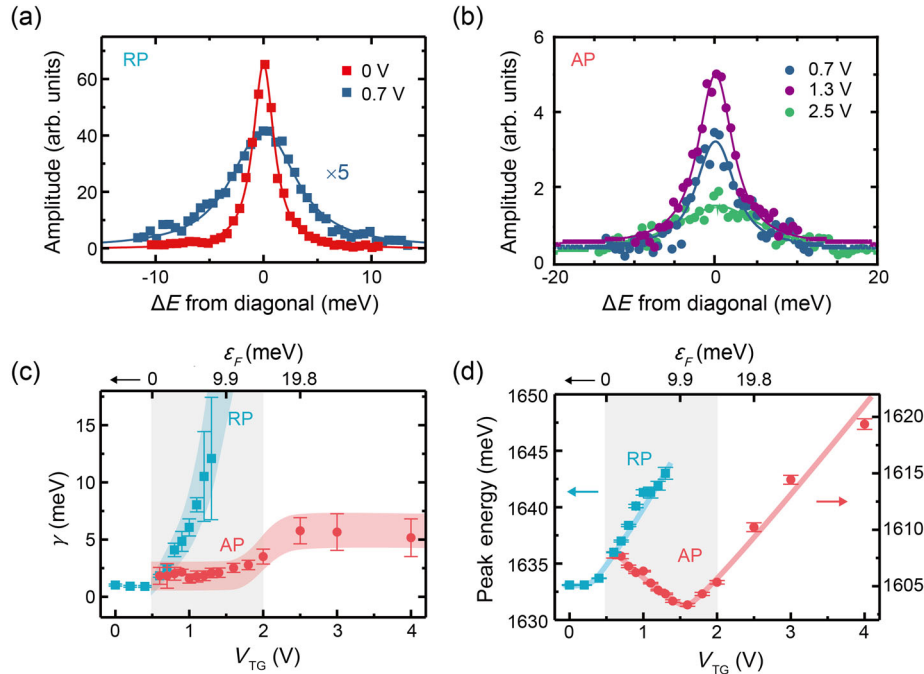


FIG. 3. Homogeneous linewidths and resonant energies of APs and RPs extracted from 2D spectra. Cross-diagonal line cuts of 2D spectra used to extract homogeneous linewidths for (a) RPs and (b) APs at a few selected top-gate voltages. The data points are fitted by a modified Voigt function as discussed in the Supplemental Material [21]. (c) Homogeneous linewidths and (d) resonant energy of RPs (blue) and APs (red) as a function of the top-gate voltage (bottom x axis) and corresponding Fermi levels (top x axis). The shaded gray area indicates the doping density range over which the polaron theory applies.

decoherence rate of APs remains largely constant until the doping density exceeds a critical density at $V_{\text{TG}} = 1.5$ V as shown in Fig. 3(c) (red curve) ($\gamma = 1.87 \pm 1.06$, 2.08 ± 0.41 , and 5.77 ± 1.14 meV with $V_{\text{TG}} = 0.7$, 1.3 and 2.5 V, respectively). Figure 3(d) displays the central energies of the APs (red points) and RPs (blue points) which are extracted from fitting to the inhomogeneous slices along the diagonal direction of the 2D spectra (details in Supplemental Material Figs. S5 and S6 [21]). In the range of gate voltages that correspond to a modest doping density, a continuous redshift of the AP resonance is observed, suggesting the coherent dressing of the quasiparticle can lower its energy. The redshift of the APs against the doping level is often overlooked or left unexplained in previous studies [26]. By contrast, the energy of the RP exhibits a blueshift over the whole doping range in which this resonance is observable in the 2DCES spectra. Interestingly, the energy of the APs begins to blueshift at a critical density that approximately coincides with where the quantum dephasing rate starts to increase.

III. DISCUSSION AND CONCLUSION

Remarkably, most of the key experimental observations (doping-dependent energy, oscillator strength, and quantum decoherence rate) can be well captured by a microscopic theory based on the simple Chevy ansatz [27] of Fermi

polarons. The excess electrons have two main effects: exciton renormalization and polaronic dressing [8]. The former modifies the resonance frequency and oscillator strength of excitons, but it does not lead to polaron formation or two separate branches. These excitons interact with excess electrons, and the polaronic dressing splits them into AP and RP branches. The polaronic physics is solely responsible for the relative behavior of the two branches (i.e., the relative frequency, broadening, and the oscillator strength), which is the focus of the present paper. As illustrated in Fig. 4(a), an exciton polaron ($P_{\mathbf{q}}^{\dagger}$) represents the coherent superposition of the undressed exciton ($X_{\mathbf{q}}^{\dagger}$ with weight $\phi_{\mathbf{q}}$) and the polaron cloud, which is approximated as a single-electron-hole excitation of the opposite valley to that in which the exciton resides ($f_{\mathbf{k}}^{\dagger}f_{\mathbf{k}'}$ in the Fermi sea with weight $\chi_{\mathbf{q}\mathbf{k}\mathbf{k}'}$ and momenta $k > k_F$ and $k' < k_F$):

$$P_{\mathbf{q}}^{\dagger} = \phi_{\mathbf{q}}X_{\mathbf{q}}^{\dagger} + \sum_{\mathbf{k}\mathbf{k}'} \chi_{\mathbf{q}\mathbf{k}\mathbf{k}'} X_{\mathbf{q}+\mathbf{k}'-\mathbf{k}}^{\dagger} f_{\mathbf{k}}^{\dagger} f_{\mathbf{k}'}. \quad (1)$$

As sketched in Figs. 1(b) and 4(b), the exciton and the unbound electron-hole excitation responsible for the polaronic dressing reside in different valleys in our microscopic theory, since same-valley correlations are suppressed by exchange effects due to the indistinguishability

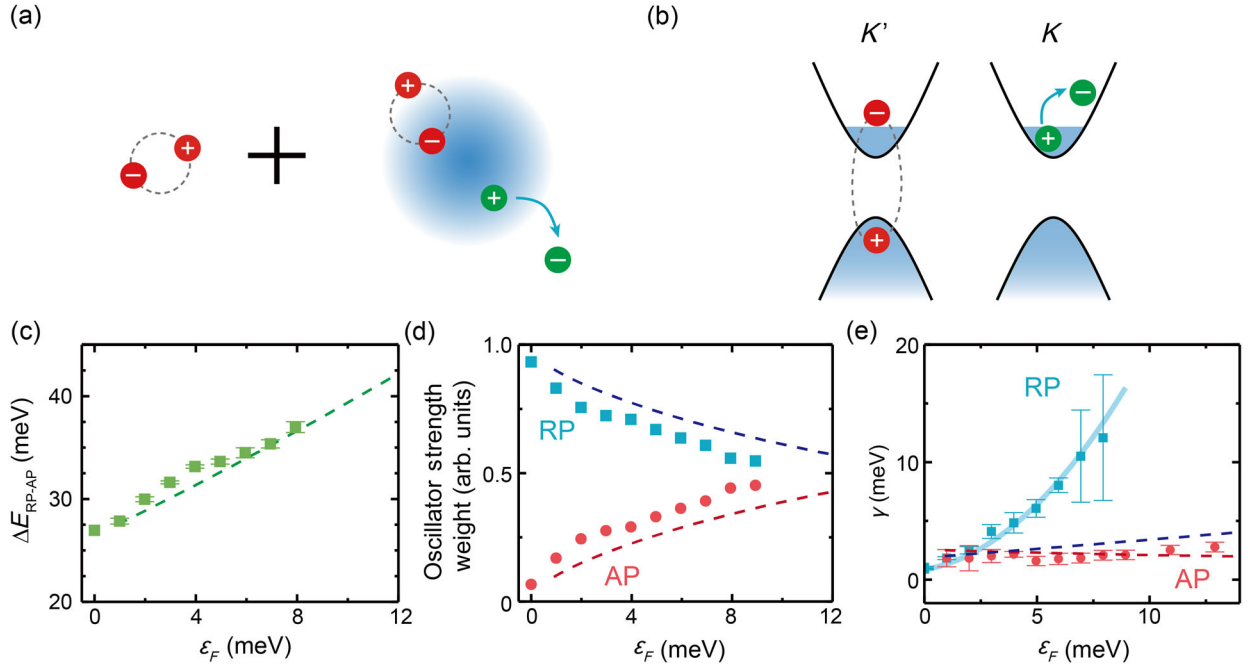


FIG. 4. Polaron theory and comparison with experiments. (a) The exciton polaron is the coherent superposition of a bare exciton and an exciton dressed by a polaron cloud approximated by a single Fermi sea (FS) unbound electron-hole pair in momentum space. (b) Exciton and the FS pair are assumed to reside in different valleys. In panels (a) and (b), red spheres refer to electrons (−) and holes (+) in one valley, while green spheres indicate those in the opposite valley. Comparisons between measurements and calculations for (c) energy splitting between APs and RPs, (d) relative oscillator strengths, and (e) homogeneous linewidths of APs and RPs as a function of the Fermi level. In panels (c)–(e), the dashed lines indicate calculations, while solid points are extracted from 2D spectra.

between the electron bound in the exciton and those in the Fermi sea [28].

The comparisons between experimental observations and predictions from the Fermi-polaron theory are summarized in Figs. 4(c)–4(e). A hallmark of the Fermi-polaron theory in 2D is a linear increase of the energy splitting between APs and RPs ($\Delta E_{\text{RP-AP}}$) as a function of the Fermi energy as $\Delta E_{\text{RP-AP}} = \varepsilon_T + 3\varepsilon_F/2$ where ε_T is the binding energy of the exciton-electron bound state (i.e., the trion) and is treated as a fitting parameter. The prefactor 3/2 originates from the inverse reduced exciton-electron mass $2m_e/3$ in TMDCs [29], and is a signature of a mobile impurity. The experimentally extracted energy splitting matches the prediction remarkably well [Fig. 4(d)] including the slope of the linear dependence [30]. The parameters used in the analysis of experimental data are discussed in detail in Supplemental Material [21], in particular, ε_T is estimated to be approximately 26.9 meV in our fitting. We further analyze the relative oscillator strength transfer between the APs (f_{AP}) and RPs (f_{RP}) as a function of the Fermi level. The oscillator strength of both APs and RPs is evaluated by integrating the amplitude over the area (labeled as S_{AP} and S_{RP}) around the resonances in the 2DCES spectra (details in Supplemental Material [21]). An excellent agreement is found between our measurements and the prediction of the polaron theory in Fig. 4(e). Note that the oscillator strength of the AP peak vanishes as the Fermi energy goes to zero, while the energy splitting between branches remains finite and reduces to the trion binding energy. Moreover, for low doping $\varepsilon_F \lesssim 2$ meV, the trion and polaron pictures give equivalent results for the oscillator strength [13].

Another key prediction of the Fermi-polaron theory is that the AP linewidth is almost doping independent, which agrees well with the experimental observation up to $\varepsilon_F \sim 15$ meV [Fig. 4(d)]. This behavior cannot be captured within the trion picture, which instead predicts that the AP linewidth increases approximately linearly with ε_F [13,31]. However, the polaron theory substantially underestimates the observed RP broadening as doping density increases. This observation is in sharp contrast to the situation in ultracold atomic gases, where the Chevy ansatz accurately describes the RP linewidth [32]. The observed RP linewidth is very well fitted by adding an extra quadratic term to the linear dependence on ε_F predicted by the polaron theory [blue solid line in Fig. 4(e)]. This discrepancy suggests the existence of a qualitatively new contribution to RP decay. The quadratic dependence of the additional broadening hints at the involvement of electron-electron interactions. In particular, the additional RP decay can originate from non-radiative transitions from the RP to the AP. Although we cannot rule out phonons and charge fluctuations as possible contributing factors to dephasing, they are anticipated to affect both polaronic branches in similar

ways, making them unlikely reasons for different doping-dependent dephasing. The decay due to electron-electron interactions involves an extra particle-hole pair that carries away the energy difference between the branches, leading to a six-particle final state that is not included in the Chevy ansatz. This decay process is enhanced when the Fermi-sea pair is in the same valley as the exciton since this avoids Pauli blocking effects with the dressing cloud.

We estimate the nonradiative decay from RPs to APs using Fermi's golden rule:

$$\gamma_{ee} = \pi \sum_{\mathbf{q}\mathbf{k}'} |\langle f | \hat{H}_{e-e} | i \rangle|^2 \times \delta(\Delta E_{\text{RP-AP}} - \varepsilon_{\mathbf{q}}^X - \varepsilon_{\mathbf{k}'-\mathbf{q}}^e + \varepsilon_{\mathbf{k}'}^e). \quad (2)$$

Here, $|i\rangle = P_{\mathbf{0},R}^\dagger |g\rangle$ is the initial RP state, while the final state $|f\rangle = P_{\mathbf{q},A}^\dagger \tilde{f}_{\mathbf{k}'-\mathbf{q}}^\dagger \tilde{f}_{\mathbf{k}'} |g\rangle$ includes an electron-hole excitation ($|\mathbf{k}' - \mathbf{q}| > k_F$ and $|\mathbf{k}'| < k_F$) that is distinguishable from that participating in the polaron state described by Eq. (1). We neglect short-range exciton-exciton and exciton-electron interactions and keep only the dominant long-range electron-electron Coulomb interactions in \hat{H}_{e-e} . The energy conservation is determined by the energy difference $\Delta E_{\text{RP-AP}}$ between the zero-momentum RP and AP states, the dispersion of the AP in the final state which can be approximated by the bare exciton dispersion $\varepsilon_{\mathbf{k}}^X$, and the energy associated with an electron-hole excitation in terms of the electron dispersion $\varepsilon_{\mathbf{k}}^e$. As presented in the Supplemental Material [21], the additional broadening can be written as

$$\gamma_{ee} \approx \frac{3\pi M^2 \varepsilon_F^2 \varepsilon_X}{4 \varepsilon_T^2}. \quad (3)$$

Here, ε_X is the binding energy for excitons. The dimensionless constant M describes the overlap between polaronic clouds in the initial and final states (details in Supplemental Material [21]). M is largely independent of doping density and is used as a fitting parameter. Most importantly, this extra contribution is proportional to ε_F^2 . When it is combined with the linear doping dependence from the Chevy ansatz, the experimental data can be fitted well.

Examples of accurate theory for strongly interacting many-body systems are rare. In this work, we demonstrate how the Fermi-polaron theory can be used to describe the quantum dynamics of an imbalanced quantum mixture of excitons and an electron gas in a MoSe₂ monolayer. While Fermi polarons in the cold-atom systems and 2D semiconductors share similar properties, e.g., the linear RP-AP energy splitting and stable quantum dynamics of APs as a function of the Fermi level [2], there are also important differences. The quantum dephasing rate of RPs increases quadratically with the doping density in TMDC monolayers in contrast to the linear dependence found in

cold-atom systems [33]. The additional broadening is intricately connected with the rich and complicated interplay of two valleys that is present not only in MoSe₂, but in all TMDC monolayer semiconductors. Our study demonstrates another fruitful playground to study the Fermi-polaron problem complementary to cold atoms where this problem has been investigated intensely in recent years [5,33–35]. The understanding of Fermi polarons in monolayers also provides a foundation for exploring the coupling between excitons and other correlated electronic ground states such as Wigner crystals, Mott insulating states, and superconductivitylike states in doped TMDC twisted bilayers [36].

ACKNOWLEDGMENTS

The spectroscopic experiments performed by D. H. and K. S. at UT Austin were primarily supported by the Department of Energy, Basic Energy Science program via Grant No. DE-SC0019398, and N. Y. is partially supported by NSF Grant No. DMR-1808042. The work was partly done at the Texas Nanofabrication Facility supported by NSF Grant No. NNCI-2025227. K. S. acknowledges a fellowship via NSF Grant No. DMR-1747426 and partial support from the NSF MRSEC Program No. DMR-1720595, which also supports the facility for preparing the sample. X. L. gratefully acknowledges sample preparation support by the Welch Foundation via Grant No. F-1662. H. L. acknowledges support by NSF via Grant No. DMR-2122078. J. L., D. K. E., and M. M. P. acknowledge support from the Australian Research Council Centre of Excellence in Future Low-Energy Electronics Technologies (Grant No. CE170100039). J. L. and M. M. P. are also supported through the ARC Future Fellowship Grants No. FT160100244 and No. FT200100619, respectively, and J. L. furthermore acknowledges support from the ARC Discovery Project No. DP210101652. E. T. acknowledges support from the Army Research Office Grant No. W911NF-17-1-0312, and the NSF MRSEC Program No. DMR-1720595. K. W. and T. T. acknowledge support from JSPS KAKENHI (Grants No. 19H05790, No. 20H00354, and No. 21H05233).

D. H., K. S., and Y. N. contributed equally to this work.

-
- [1] P. Massignan, M. Zaccanti, and G. M. Bruun, *Polarons, Dressed Molecules and Itinerant Ferromagnetism in Ultracold Fermi Gases*, *Rep. Prog. Phys.* **77**, 034401 (2014).
 [2] J. Levinsen and M. M. Parish, *Strongly Interacting Two-Dimensional Fermi Gases*, in *Annual Review of Cold Atoms and Molecules* (World Scientific, 2015), Chap. 1, pp. 1–75, [10.1142/9789814667746_0001](https://doi.org/10.1142/9789814667746_0001).
 [3] M. Cetina, M. Jag, R. S. Lous, I. Fritsche, J. T. M. Walraven, R. Grimm, J. Levinsen, M. M. Parish, R. Schmidt, M. Knap,

- and E. Demler, *Ultrafast Many-Body Interferometry of Impurities Coupled to a Fermi Sea*, *Science* **354**, 96 (2016).
 [4] A. Schirotzek, C.-H. Wu, A. Sommer, and M. W. Zwierlein, *Observation of Fermi Polarons in a Tunable Fermi Liquid of Ultracold Atoms*, *Phys. Rev. Lett.* **102**, 230402 (2009).
 [5] C. Kohstall, M. Zaccanti, M. Jag, A. Trenkwalder, P. Massignan, G. M. Bruun, F. Schreck, and R. Grimm, *Metastability and Coherence of Repulsive Polarons in a Strongly Interacting Fermi Mixture*, *Nature (London)* **485**, 615 (2012).
 [6] S. Nascimbène, N. Navon, K. J. Jiang, L. Tarruell, M. Teichmann, J. McKeever, F. Chevy, and C. Salomon, *Collective Oscillations of an Imbalanced Fermi Gas: Axial Compression Modes and Polaron Effective Mass*, *Phys. Rev. Lett.* **103**, 170402 (2009).
 [7] J. B. McGuire, *Interacting Fermions in One Dimension. II. Attractive Potential*, *J. Math. Phys.* **7**, 123 (1966).
 [8] M. Sidler, P. Back, O. Cotlet, A. Srivastava, T. Fink, M. Kroner, E. Demler, and A. Imamoglu, *Fermi Polaron-Polaritons in Charge-Tunable Atomically Thin Semiconductors*, *Nat. Phys.* **13**, 255 (2017).
 [9] D. K. Efimkin and A. H. MacDonald, *Many-Body Theory of Trion Absorption Features in Two-Dimensional Semiconductors*, *Phys. Rev. B* **95**, 035417 (2017).
 [10] T. Mueller and E. Malic, *Exciton Physics and Device Application of Two-Dimensional Transition Metal Dichalcogenide Semiconductors*, *npj 2D Mater. Appl.* **2**, 29 (2018).
 [11] M. He, P. Rivera, D. Van Tuan, N. P. Wilson, M. Yang, T. Taniguchi, K. Watanabe, J. Yan, D. G. Mandrus, H. Yu, H. Dery, W. Yao, and X. Xu, *Valley Phonons and Exciton Complexes in a Monolayer Semiconductor*, *Nat. Commun.* **11**, 618 (2020).
 [12] K. F. Mak, K. He, C. Lee, G. H. Lee, J. Hone, T. F. Heinz, and J. Shan, *Tightly Bound Trions in Monolayer MoS₂*, *Nat. Mater.* **12**, 207 (2013).
 [13] M. M. Glazov, *Optical Properties of Charged Excitons in Two-Dimensional Semiconductors*, *J. Chem. Phys.* **153**, 034703 (2020).
 [14] R. Suris, V. Kochereshko, G. Astakhov, D. Yakovlev, W. Ossau, J. Nürnberger, W. Faschinger, G. Landwehr, T. Wojtowicz, G. Karczewski, and J. Kossut, *Excitons and Trions Modified by Interaction with a Two-Dimensional Electron Gas*, *Phys. Status Solidi (b)* **227**, 343 (2001).
 [15] S.-Y. Shiao, M. Combescot, and Y.-C. Chang, *Trion Ground State, Excited States, and Absorption Spectrum Using Electron-Exciton Basis*, *Phys. Rev. B* **86**, 115210 (2012).
 [16] M. Baeten and M. Wouters, *Many-Body Effects of a Two-Dimensional Electron Gas on Trion-Polaritons*, *Phys. Rev. B* **91**, 115313 (2015).
 [17] J. Li, M. Goryca, J. Choi, X. Xu, and S. A. Crooker, *Many-Body Exciton and Intervalley Correlations in Heavily Electron-Doped WSe₂ Monolayers*, *Nano Lett.* **22**, 426 (2022).
 [18] K. Wagner, E. Wietek, J. D. Ziegler, M. A. Semina, T. Taniguchi, K. Watanabe, J. Zipfel, M. M. Glazov, and A. Chernikov, *Autoionization and Dressing of Excited Excitons by Free Carriers in Monolayer WSe₂*, *Phys. Rev. Lett.* **125**, 267401 (2020).

- [19] D. Van Tuan, S.-F. Shi, X. Xu, S. A. Crooker, and H. Dery, *Hexcitons and Oxcitons in Monolayer WSe₂*, [arXiv:2202.08375](https://arxiv.org/abs/2202.08375).
- [20] T. Smoleński, O. Cotlet, A. Popert, P. Back, Y. Shimazaki, P. Knüppel, N. Dietler, T. Taniguchi, K. Watanabe, M. Kroner, and A. Imamoglu, *Interaction-Induced Shubnikov-de Haas Oscillations in Optical Conductivity of Monolayer MoSe₂*, *Phys. Rev. Lett.* **123**, 097403 (2019).
- [21] See Supplemental Material at <http://link.aps.org/supplemental/10.1103/PhysRevX.13.011029> for additional information about (1) 2DCES experiment, (2) exciton-polaron theory, (3) nonradiative broadening of repulsive polarons, (4) device fabrication, (5) polaron energy splitting vs Fermi energy, (6) methods to extract γ and resonant energy, (7) method to evaluate relative oscillator strength, and (8) exciton and temperature broadening effect.
- [22] M. E. Siemens, G. Moody, H. Li, A. D. Bristow, and S. T. Cundiff, *Resonance Lineshapes in Two-Dimensional Fourier Transform Spectroscopy*, *Opt. Express* **18**, 17699 (2010).
- [23] G. Moody, C. Kavir Dass, K. Hao, C. H. Chen, L. J. Li, A. Singh, K. Tran, G. Clark, X. Xu, G. Berghauser, E. Malic, A. Knorr, and X. Li, *Intrinsic Homogeneous Linewidth and Broadening Mechanisms of Excitons in Monolayer Transition Metal Dichalcogenides*, *Nat. Commun.* **6**, 8315 (2015).
- [24] E. W. Martin, J. Horng, H. G. Ruth, E. Paik, M.-H. Wentzel, H. Deng, and S. T. Cundiff, *Encapsulation Narrows and Preserves the Excitonic Homogeneous Linewidth of Exfoliated Monolayer MoSe₂*, *Phys. Rev. Appl.* **14**, 021002(R) (2020).
- [25] K. Hao, L. Xu, P. Nagler, A. Singh, K. Tran, C. K. Dass, C. Schüller, T. Korn, X. Li, and G. Moody, *Coherent and Incoherent Coupling Dynamics between Neutral and Charged Excitons in Monolayer MoSe₂*, *Nano Lett.* **16**, 5109 (2016).
- [26] E. Liu, J. Van Baren, Z. Lu, T. Taniguchi, K. Watanabe, D. Smirnov, Y.-C. Chang, and C. H. Lui, *Exciton-Polaron Rydberg States in Monolayer MoSe₂ and WSe₂*, *Nat. Commun.* **12**, 6131 (2021).
- [27] F. Chevy, *Universal Phase Diagram of a Strongly Interacting Fermi Gas with Unbalanced Spin Populations*, *Phys. Rev. A* **74**, 063628 (2006).
- [28] A. Tienne, J. Levinsen, J. Keeling, M. M. Parish, and F. M. Marchetti, *Effect of Fermion Indistinguishability on Optical Absorption of Doped Two-Dimensional Semiconductors*, *Phys. Rev. B* **105**, 125404 (2022).
- [29] D. K. Efimkin, E. K. Laird, J. Levinsen, M. M. Parish, and A. H. MacDonald, *Electron-Exciton Interactions in the Exciton-Polaron Problem*, *Phys. Rev. B* **103**, 075417 (2021).
- [30] Our calculations follow Ref. [9]. In the recent paper [29], exciton-electron interactions and the binding energy ϵ_T are calculated microscopically, and ϵ_T reasonably agrees with the trion binding energy evaluated within the genuine three-particle problem. Importantly, the doping dependence of absorption calculated within the two models (with microscopically derived interactions and ones approximated by the contact pseudopotential) are very close to each other.
- [31] C. Zhang, H. Wang, W. Chan, C. Manolatu, and F. Rana, *Absorption of Light by Excitons and Trions in Monolayers of Metal Dichalcogenide MoS₂: Experiments and Theory*, *Phys. Rev. B* **89**, 205436 (2014).
- [32] H. S. Adlong, W. E. Liu, F. Scazza, M. Zaccanti, N. D. Oppong, S. Fölling, M. M. Parish, and J. Levinsen, *Quasi-particle Lifetime of the Repulsive Fermi Polaron*, *Phys. Rev. Lett.* **125**, 133401 (2020).
- [33] N. Darkwah Oppong, L. Riegger, O. Bettermann, M. Höfer, J. Levinsen, M. M. Parish, I. Bloch, and S. Fölling, *Observation of Coherent Multiorbital Polarons in a Two-Dimensional Fermi Gas*, *Phys. Rev. Lett.* **122**, 193604 (2019).
- [34] M. Koschorreck, D. Pertot, E. Vogt, B. Fröhlich, M. Feld, and M. Köhl, *Attractive and Repulsive Fermi Polarons in Two Dimensions*, *Nature (London)* **485**, 619 (2012).
- [35] F. Scazza, G. Valtolina, P. Massignan, A. Recati, A. Amico, A. Burchianti, C. Fort, M. Inguscio, M. Zaccanti, and G. Roati, *Repulsive Fermi Polarons in a Resonant Mixture of Ultracold ⁶Li atoms*, *Phys. Rev. Lett.* **118**, 083602 (2017).
- [36] T. Smoleński, P. E. Dolgirev, C. Kuhlenkamp, A. Popert, Y. Shimazaki, P. Back, X. Lu, M. Kroner, K. Watanabe, T. Taniguchi, I. Esterlis, E. Demler, and A. Imamoglu, *Signatures of Wigner Crystal of Electrons in a Monolayer Semiconductor*, *Nature (London)* **595**, 53 (2021).